

# Supplementary Information

## Rewiring and Dosing of Systems Modules as Engineering Approach for Designing Synthetic Mammalian Gene Networks

Michael M. Kämpf, Raphael Engesser, Moritz Busacker,  
Maximilian Hörner, Maria Karlsson, Matias D. Zurbriggen,  
Martin Fussenegger, Jens Timmer and Wilfried Weber

### Table of Contents

1. Derivation of a quantitative ODE model for auxin-based band-detect system .....	2
2. Multi-experiment fit of low-, high- and band-detect filter with target gene SEAP.	10
3. Expanding the network .....	16
3.1. Auxin-responsive band-detect filter based on ScbR.....	16
3.2. Biotin-responsive band-detect filter.....	17
3.3. Two-dimensional gradients with the auxin-dependent band detect system.....	18
3.4. Additive superposition of biotin- and auxin-dependent band-detect filters.....	19
3.5. Conjunction-type connection of the biotin- and auxin-responsive band-detect networks.....	20
3.6. Direct rewiring of the auxin-responsive low-detect filter with the biotin- responsive band-detect network.....	20
4. Auxin and biotin gradients.....	23
5. Supplementary Figures .....	25
6. Supplementary Data Tables .....	29
7. Supplementary References.....	33

## 1. Derivation of a quantitative ODE model for auxin-based band-detect system

The auxin-based band-detect system consists of different modules on different levels. On the one hand there is the hormone level where the hormone auxin is binding to the constitutively expressed receptor TIR1 to a complex C. The total TIR1 amount is assumed as constant, which means the production and degradation of TIR1 is in equilibrium. The auxin-TIR1 complex C is inducing the ubiquitination of the AID-fused proteins of the high-detect and low-detect filter modules. The complex formation is reversible



This simple reaction system is described by the equations

$$\frac{d[\text{AUX}]}{dt} = k^-[\text{C}] - k^+[\text{AUX}][\text{TIR1}] \quad (\text{S2a})$$

$$\frac{d[\text{TIR1}]}{dt} = k^-[\text{C}] - k^+[\text{AUX}][\text{TIR1}] \quad (\text{S2b})$$

$$\frac{d[\text{C}]}{dt} = -k^-[\text{C}] + k^+[\text{AUX}][\text{TIR1}]. \quad (\text{S2c})$$

On the other hand there is the high-detect module and the low-detect module based on gene expression. In the low-detect filter module, tTA-AID is expressed by the  $P_{\text{TET}}$  promoter that is responsive to tTA-AID. tTA-AID is degraded by the auxin-TIR1 complex from the hormone level. In the high-detect filter module, E-KRAB-AID is produced constitutively and also degraded by the auxin-TIR1 complex. The target gene SEAP is under control of the transcription factor tTA-AID and the allosteric inhibitor E-KRAB-AID.

To quantitatively describe the expression of a gene A under the control of a transcription factor the equation

$$\frac{d[A]}{dt} = b + k \frac{[T]^n}{K_m^n + [T]^n}. \quad (\text{S3})$$

can be used (Karlebach & Shamir, 2008). The basal production rate  $b$  is due to leakiness of the promoter. The second term is describing the activation process. It is similar to a Monod kinetic with a Hill coefficient  $n$  which depends on the cooperative binding of the transcription factor to the promoter. If the basal production is zero,  $k$  is the maximum expression rate. It is proportional to the promoter strength and to the promoter concentration. The gene expression is saturating in respect to the transactivator  $T$ , this is described by the Monod constant  $K_m$ . For  $[T] = K_m$  the expression rate is  $b + \frac{k}{2}$ . This simple model to describe gene expression merges the transcription and the translation step to one single ordinary differential equation. If the concentration of the transcription factor is constant the right-hand side of eq. (S3) is constant and the gene A is expressed with a constant rate rate  $b_c$

$$\frac{d[A]}{dt} = b_c. \quad (\text{S4})$$

The ubiquitination of tTA-AID and E-KRAB-AID can be described by enzyme kinetics, e.g. for tTA-AID:



The auxin-TIR1 complex  $C$  is acting as enzyme that induces the ubiquitination. The role of tTA-AID is similar to a substrate and the products of decomposition  $P$  are not influencing the system anymore. The changing of tTA-AID is described by Michaelis-Menten kinetics

$$\frac{d[\text{tTA-AID}]}{dt} = -k_d \frac{[C][\text{tTA-AID}]}{K_{deg} + [\text{tTA-AID}]}. \quad (\text{S6})$$

If  $[\text{tTA-AID}] \ll K_{deg}$  one can approximate eq. (S6) linearly

$$\frac{d[\text{tTA-AID}]}{dt} = -k_3 [C][\text{tTA-AID}] \quad (\text{S7})$$

with  $k_3 = k_d/K_{deg}$ . Additionally every protein is degraded linear with a certain rate and we have to modify eq. (S7) to

$$\frac{d[tTA-AID]}{dt} = -k_1[tTA-AID] - k_3[C][tTA-AID]. \quad (S8)$$

For the degradation of E-KRAB-AID follows analogously

$$\frac{d[E-KRAB-AID]}{dt} = -k_4[E-KRAB-AID] - k_5[C][E-KRAB-AID]. \quad (S9)$$

The production of the target gene SEAP under the control of the  $P_{Hybrid}$  promoter is described by the equation

$$\frac{d[SEAP]}{dt} = b_3 + \frac{k_6}{1+k_7[E-KRAB-AID]^2} \frac{[tTA-AID]^2}{K_{m2}^2 + [tTA-AID]^2}. \quad (S10)$$

SEAP is activated by the transcription factor tTA-AID described by Monod kinetics. As Hill coefficient we use  $n = 2$  because tTA-AID binds as dimer cooperatively to the promoter. The allosteric inhibition of E-KRAB-AID is described by the term  $1 + k_7[E-KRAB-AID]^2$  in the denominator, the square is due to the cooperative binding of E-KRAB-AID dimers to the  $P_{Hybrid}$  promoter. The  $P_{Hybrid}$  promoter has eight independent binding sites for the E-KRAB-AID dimers, since the binding is non-cooperative, this has only an impact on the parameter  $k_7$  (Fussenegger et al, 2000; Kramer et al, 2004). SEAP is very stable, thus we can neglect the linear degradation rate.

Summarized we obtain a first ODE model:

$$\frac{d[tTA-AID]}{dt} = b_1 - (k_1 + k_3[C])[tTA-AID] + k_2 \frac{[tTA-AID]^2}{K_{m1}^2 + [tTA-AID]^2} \quad (S11a)$$

$$\frac{d[E-KRAB-AID]}{dt} = b_2 - (k_4 + k_5[C])[E-KRAB-AID] \quad (S11b)$$

$$\frac{d[AUX]}{dt} = k^- [C] - k^+ [AUX][TIR1] \quad (S11c)$$

$$\frac{d[TIR1]}{dt} = k^- [C] - k^+ [AUX][TIR1] \quad (S11d)$$

$$\frac{d[C]}{dt} = -k^- [C] + k^+ [AUX][TIR1] \quad (S11e)$$

$$\frac{d[SEAP]}{dt} = b_3 + \frac{k_6}{1+k_7[E-KRAB-AID]^2} \frac{[tTA-AID]^2}{K_{m2}^2 + [tTA-AID]^2} \quad (S11f)$$

The binding of the hormone auxin to TIR1 takes place very fast, because  $k^+$  and  $k^-$  in the reaction (S1) are very large in comparison to the time scales of the gene expression-dependent processes. Thus, we can assume that the reaction is in a chemical equilibrium. To find the equilibrium concentration  $[C]_{eq}$  of C depending on the initial concentration of auxin and of TIR1 one can use the law of mass action:

$$K = \frac{[AUX]_{eq} [TIR1]_{eq}}{[C]_{eq}} \quad (S12)$$

The ratio of the educts and the product is constant,  $K := \frac{k_-}{k_+}$  is the dissociation constant of the reaction. With mass conservation we can make the substitutions  $[AUX]_{eq} = [AUX]_0 - [C]_{eq}$  and  $[TIR1]_{eq} = [TIR1]_0 - [C]_{eq}$ . This leads to a quadratic equation for the steady state concentration of the complex  $[C]_{eq}$ :

$$[C]_{eq}^2 - ([Aux]_0 + [TIR1]_0 + K)[C]_{eq} + [Aux]_0[TIR1]_0 = 0 \quad (S13)$$

The solution of this equation is

$$[C]_{eq_{1/2}} = \frac{[AUX]_0 + [TIR1]_0 + K}{2} \pm \sqrt{\left(\frac{[AUX]_0 + [TIR1]_0 + K}{2}\right)^2 - [AUX]_0 [TIR1]_0} \quad (S14a)$$

For  $[C]_{eq_1}$  is  $[TIR1]_{eq}$ ,  $[AUX]_{eq} < 0$  which means that

$$[C]_{eq_2} = \frac{[AUX]_0 + [TIR1]_0 + K}{2} - \sqrt{\left(\frac{[AUX]_0 + [TIR1]_0 + K}{2}\right)^2 - [AUX]_0 [TIR1]_0} \quad (S14b)$$

is the unique equilibrium concentration of the TIR1-auxin complex C depending on the initial concentrations  $[AUX]_0$  and  $[TIR1]_0$  and the dissociation constant  $K$ .

The acting auxin concentration in the nucleus is less than the auxin concentration in the medium outside the cells. To describe this in the model we have to introduce a factor  $f$  in eq. (S14b) that describes the fraction of the auxin concentration in the nucleus to the auxin concentration in the medium:

$$[C]_{eq} = \frac{f[AUX]_0 + [TIR1]_0 + K}{2} - \sqrt{\left(\frac{f[AUX]_0 + [TIR1]_0 + K}{2}\right)^2 - f[AUX]_0 [TIR1]_0} \quad (S15)$$

With this we obtain for the auxin-dependent band-detect filter the following ODE model:

$$\frac{d[tTA-AID]}{dt} = b_1 - (k_1 + k_3[C]_{eq})[tTA-AID] + k_2 \frac{[tTA-AID]^2}{K_{m1}^2 + [tTA-AID]^2} \quad (S16a)$$

$$\frac{d[E-KRAB-AID]}{dt} = b_2 - (k_4 + k_5[C]_{eq})[E-KRAB-AID] \quad (S16b)$$

$$\frac{d[SEAP]}{dt} = b_3 + \frac{k_6}{1 + k_7[E-KRAB-AID]^2} \frac{[tTA-AID]^2}{K_{m2}^2 + [tTA-AID]^2} \quad (S16c)$$

$$\text{with } [C]_{eq} = \frac{f[AUX]_0 + [TIR1]_0 + K}{2} - \sqrt{\left(\frac{f[AUX]_0 + [TIR1]_0 + K}{2}\right)^2 - f[AUX]_0 [TIR1]_0}$$

To obtain the models of the single low- and high-detect filter we only have to modify the equation for the target gene SEAP. As model for the low-detect filter we get

$$\frac{d[tTA-AID]}{dt} = b_1 - (k_1 + k_3[C]_{eq})[tTA-AID] + k_2 \frac{[tTA-AID]^2}{K_{m1}^2 + [tTA-AID]^2} \quad (S16a)$$

$$\frac{d[SEAP]}{dt} = b_3 + k_6 \frac{[tTA-AID]^2}{K_{m2}^2 + [tTA-AID]^2}, \quad (S17)$$

and for the high-detect filter we obtain

$$\frac{d[E-KRAB-AID]}{dt} = b_2 - (k_4 + k_5[C]_{eq})[E-KRAB-AID] \quad (S16b)$$

$$\frac{d[SEAP]}{dt} = \frac{b_4}{1 + k_7[E-KRAB-AID]^2} \quad (S18)$$

In the high-detect filter the constitutive expression of the target gene SEAP is inhibited by E-KRAB-AID.

## Freedom in scaling

The target gene SEAP is the output of the system that is measured.  $[tTA-AID]$  and  $[E-KRAB-AID]$  are internal variables. If we change the scale of  $[tTA-AID]$  and  $[E-KRAB-AID]$  by a factor  $\alpha$ , we can compensate this by changing the parameters  $k_7 \longrightarrow k'_7 = k_7/\alpha^2$  and  $K_{m2} \longrightarrow K'_{m2} = K_{m2} \alpha$  in eq. (S16c). This means the scale of  $[tTA-AID]$  and  $[E-KRAB-AID]$  is not determined. One can use this freedom in choosing a scale of the internal variables to decrease the number of dynamical parameters in the model, by defining a scale for  $[tTA-AID]$  and  $[E-KRAB-AID]$  which depends on parameters of the system.

Consider eq. (S16b)

$$\frac{d[E-KRAB-AID]}{dt} = b_2 - (k_4 + k_5[C]_{eq})[E-KRAB-AID] \quad (\text{S16b})$$

Without auxin, the equilibrium concentration of the auxin-TIR1 complex is  $[C]_{eq} = 0$  and in equilibrium we obtain

$$0 = \frac{d[E-KRAB-AID]}{dt} = b_2 - k_4[E-KRAB-AID]. \quad (\text{S19})$$

Thus the steady state concentration of  $[E-KRAB-AID]$  in absence of any auxin is  $[E-KRAB-AID]_0 = b_2/k_4$ . We can use this concentration  $[E-KRAB-AID]_0$  as unit of  $[E-KRAB-AID]$ . This is done by rescaling  $[E-KRAB-AID] \longrightarrow [E-KRAB-AID]' = [E-KRAB-AID]/[E-KRAB-AID]_0$  and  $k_7 \longrightarrow k'_7 = k_7[E-KRAB-AID]_0^2$  in eq. (S16C), (S17) and (S18). By dividing eq. (S16b) by the new unit  $[E-KRAB-AID]_0$  we obtain

$$\frac{\frac{d[E-KRAB-AID]}{dt}}{[E-KRAB-AID]_0} = \frac{b_2}{[E-KRAB-AID]_0} - (k_4 + k_5[C]_{eq}) \frac{[E-KRAB-AID]}{[E-KRAB-AID]_0}. \quad (\text{S20})$$

Applying the rescaling and using  $[E-KRAB-AID]_0 = b_2/k_4$  we obtain

$$\frac{d[E-KRAB-AID]'}{dt} = k_4 - (k_4 + k_5[C]_{eq})[E-KRAB-AID]'. \quad (S21)$$

$[E-KRAB-AID]'$  is now considered in units of  $[E-KRAB-AID]_0$  and the eq. (S21) has one parameter less.

To obtain the steady state concentration of  $tTA-AID$  analytically we have to solve the cubic equation

$$0 = b_1 K_{m1}^2 - k_1 K_{m1}^2 [tTA-AID] + (b_1 + k_2) [tTA-AID]^2 - k_1 [tTA-AID]^3 \quad (S22)$$

which follows from eq. (S16a). Instead of solving this cubic equation for the steady state concentration  $[tTA-AID]_0$  it is easier to use  $K_{m1}$  as unit of  $[tTA-AID]$ . Consider eq. (S16a)

$$\frac{d[tTA-AID]}{dt} = b_1 - (k_1 + k_3[C]_{eq})[tTA-AID] + k_2 \frac{[tTA-AID]^2}{K_{m1}^2 + [tTA-AID]^2}. \quad (S16a)$$

Dividing this by  $K_{m1}$  and rewriting the ratio we obtain

$$\frac{\frac{d[tTA-AID]}{dt}}{K_{m1}} = \frac{b_1}{K_{m1}} - (k_1 + k_3[C]_{eq}) \frac{[tTA-AID]}{K_{m1}} + \frac{k_2}{K_{m1}} \frac{[tTA-AID]^2/K_{m1}^2}{1 + [tTA-AID]^2/K_{m1}^2}. \quad (S23)$$

Applying the rescaling  $[tTA-AID] \longrightarrow [tTA-AID]' = [tTA-AID]/K_{m1}$ ,  $b_1 \longrightarrow b_1' = b_1/K_{m1}$ ,  $k_2 \longrightarrow k_2' = k_2/K_{m1}$  and  $K_{m2} \longrightarrow K_{m2}' = K_{m2}/K_{m1}$  we get rid of the parameter  $K_{m1}$ :

$$\frac{d[tTA-AID]'}{dt} = b_1' - (k_1 + k_3[C]_{eq})[tTA-AID]' + k_2' \frac{[tTA-AID]'^2}{1 + [tTA-AID]'^2}. \quad (S24)$$

The rescaled model of the full band-detect filter has the form

$$\frac{d[tTA-AID]'}{dt} = b_1' - (k_1 + k_3[C]_{eq})[tTA-AID]' + k_2' \frac{[tTA-AID]'^2}{1 + [tTA-AID]'^2} \quad (S25a)$$

$$\frac{d[E-KRAB-AID]'}{dt} = k_4 - (k_4 + k_5[C]_{eq})[E-KRAB-AID]' \quad (S25b)$$

$$\frac{d[SEAP]}{dt} = b_3 + \frac{k_6}{1+k_7'[E-KRAB-AID]'^2} \frac{[tTA-AID]'^2}{K_{m2}'^2 + [tTA-AID]'^2} \quad (S25c)$$

$$\text{with } [C]_{eq} = \frac{f[AUX]_0 + [TIR1]_0 + K}{2} - \sqrt{\left(\frac{f[AUX]_0 + [TIR1]_0 + K}{2}\right)^2 - f[AUX]_0 [TIR1]_0}$$

For the rescaled output of the low-detect filter we obtain

$$\frac{d[tTA-AID]'}{dt} = b_1' - (k_1 + k_3[C]_{eq})[tTA-AID]' + k_2' \frac{[tTA-AID]'^2}{1+[tTA-AID]'^2} \quad (S25a)$$

$$\frac{d[SEAP]}{dt} = b_3 + k_6 \frac{[tTA-AID]'^2}{K_{m2}'^2 + [tTA-AID]'^2}, \quad (S26)$$

and for the high-detect filter we obtain

$$\frac{d[E-KRAB-AID]'}{dt} = k_4 - (k_4 + k_5[C]_{eq})[E-KRAB-AID]' \quad (S25b)$$

$$\frac{d[SEAP]}{dt} = \frac{b_4}{1+k_7'[E-KRAB-AID]'^2}. \quad (S27)$$

## 2. Multi-experiment fit of low-, high- and band-detect filter with target gene SEAP

To connect the dynamical model to the experimental observables we can write the model eq. (S25) in the following general form

$$\frac{d\mathbf{u}(t)}{dt} = \mathbf{f}(\mathbf{u}(t), \mathbf{p}, [AUX]_0) \quad (\text{S28a})$$

$$\mathbf{y}(t) = \mathbf{g}(\mathbf{u}(t), \mathbf{s}) + \boldsymbol{\epsilon}(t). \quad (\text{S28b})$$

In this scheme  $\mathbf{u} = ([tTA-AID]', [E-KRAB-AID]', [SEAP])$  is the vector of the internal model states whose time evolution is described by the ODE system defined by the right hand side function  $\mathbf{f}$ . The ODE function  $\mathbf{f}$  depends on the dynamical parameters  $\mathbf{p}$  and the external parameter  $[AUX]_0$ . The observables are denoted with  $\mathbf{y}(t)$ . The observation function  $\mathbf{g}(\mathbf{u}(t), \mathbf{s})$  is a mapping from the internal variables  $\mathbf{u}(t)$  to the observables  $\mathbf{y}(t)$  which can be measured.  $\mathbf{s}$  are scaling or offset parameters and  $\boldsymbol{\epsilon}(t)$  is the measurement noise. To obtain a unique solution of eq. (S28a) one needs also initial concentrations  $\mathbf{u}(0)$ .

The amount of  $[SEAP]$  is determined by measuring a conversion rate of a substrate. This conversion rate is an activity with the unit  $U/L$ . The concentration of  $[SEAP]$  is proportional to this activity. Thus, the observation function is

$$g(\mathbf{u}(t), s) = s [SEAP]. \quad (\text{S29})$$

By using  $U/L$  as a unit for  $[SEAP]$  one can set the scaling parameter to  $s = 1$ . The measurement is taken at  $t = 48 h$  for different concentrations of the external input parameter  $[AUX]_0$ . As initial condition we take  $\mathbf{u}(0) = 0$ . This is reasonable because the concentration of tTA-AID, E-KRAB-AID and SEAP is zero before the cells are transfected.

Let  $n_A$  denote the number of different auxin concentrations  $[AUX]_0 = A_j$ ,  $n_{A_j}$  the number of measurements at the auxin concentration  $A_j$  and  $\sigma_j$  the measurement error of the a measurement at auxin concentration  $A_j$ .

To quantify the agreement between model prediction and experimental data we define the weighted sum of the squared residuals as an objective function

$$\chi^2(\mathbf{p}) = \sum_{j=1}^{n_A} \sum_{i=1}^{n_{A_j}} \frac{\left( [SEAP]_{A_j}^i - y(t=48 \text{ h}, \mathbf{p}, [AUX]_0=A_j) \right)^2}{\sigma_j^2}. \quad (\text{S30})$$

For fitting the model to data one has to minimize this function with respect to the parameter set  $\mathbf{p}$ . If  $\epsilon(t)$  follows a normal distribution the optimization of the least square function  $\chi^2(\mathbf{p})$  is equivalent to a maximum-likelihood estimation (Raue et al, 2009). Our data are measurements of concentrations that normally do not follow a normal distribution because concentrations have to be positive. A common distribution for concentrations is the log-normal distribution with errors proportional to the measured value (Kreutz et al, 2007; Koch, 1966). The logarithm  $\log y_i$  of log-normal distributed data  $y_i$  is normal distributed. This means by fitting with logarithmized data we obtain a maximum-likelihood estimation. A constant relative error of the log-normal distributed data  $y_i$  leads to a constant absolute error on the logarithmic scale. Thus it is not necessary to weight the residuals of the logarithmized data because they have all the same constant error. This leads us to the objective function

$$\chi_{log}^2(\mathbf{p}) = \sum_{j=1}^{n_A} \sum_{i=1}^{n_{A_j}} \left( \log \left( [SEAP]_{A_j}^i \right) - \log \left( y(t = 48 \text{ h}, \mathbf{p}, A_j) \right) \right)^2. \quad (\text{S31})$$

By minimizing this function in respect to the parameter set  $\mathbf{p}$

$$\mathbf{p}_{opt} = \arg \min_{\mathbf{p}} \chi_{log}^2(\mathbf{p}) \quad (\text{S32})$$

one obtains a maximum likelihood estimation for the optimal parameter set  $\mathbf{p}_{opt}$ .

Because we have many different experiments with different systems (band-, low-, high-detect filter) and experiments with different plasmids amounts (Figure 2 and 3) we have to perform a multi-experiment fit. To take into account variations between different transfection experiments (as e.g. introduced by different cell passage

number) we introduce a scaling parameter  $s_k$  for each experiment  $k$  which scales the output  $y$  of our the model

$$y_k = s_k y. \quad (\text{S33})$$

There are two kinds of experiments. On the one hand we performed experiments for the low-, high- and band-detect filter. Since the design of the network is modular, the models have the same parameter set  $\mathbf{p}$  but different model functions  $\mathbf{f}_k$  and internal states  $\mathbf{u}_k$ . In the low-detect system the internal states are  $\mathbf{u}_{low} = ([tTA-AID]', [SEAP])$  and the dynamic is described by the function  $\mathbf{f}_{low}(\mathbf{u}(t), \mathbf{p}, [AUX]_0)$  defined by eq. (S25a) and (S26) which is depending on the same parameters  $\mathbf{p}$  than the band-detect system. In the high-detect system the internal states are  $\mathbf{u}_{high} = ([E-KRAB-AID]', [SEAP])$  and the dynamic is described by the function  $\mathbf{f}_{high}(\mathbf{u}(t), \mathbf{p}, [AUX]_0)$  defined by eq. (S25b) and (S27).

On the other hand we performed experiments with the same system but changed the properties of this system in a predefined manner. In the model this is reflected by mapping the parameter set  $\mathbf{p}$  to a modified parameter set  $\mathbf{p}_k = \mathbf{h}_k(\mathbf{p})$  while using the same model function  $\mathbf{f}$ . The function  $\mathbf{h}_k$  is determined by the experiment  $k$ . Consider the experiments in Figure 3A-C. The amount of tTA-AID and E-KRAB-AID expression plasmids were decreased to 60 % (blue) and increased to 130 % (red) of the standard plasmid amount. To model this we have to change the dynamical parameters determining the expression of tTA-AID and E-KRAB-AID. Those are  $b_1$ ,  $k_2$  and  $b_2$ . The function  $\mathbf{h}_k(\mathbf{p})$  has to map these three parameters to  $0.6 b_1$ ,  $0.6 k_2$  and  $0.6 b_2$  respectively  $1.3 b_1$ ,  $1.3 k_2$  and  $1.3 b_2$ . In Figure 3D the amount of E-KRAB-AID expression plasmids was increased 1.5-fold, therefore  $\mathbf{h}_k(\mathbf{p})$  has to map  $b_2$  to  $1.5 b_2$ . In Figure 2B the amount of the auxin receptor TIR1 was increased and decreased 3-fold compared to standard amount  $[TIR1]_0$ . The function  $\mathbf{h}_k(\mathbf{p})$  has to map the parameter  $[TIR1]_0$  to  $\frac{1}{3}[TIR1]_0$  respectively to  $3 [TIR1]_0$ .

In the objective function one has to sum additionally over all experiments  $k$

$$\chi^2(\mathbf{p}, \mathbf{s}) = \sum_{k=1}^{n_{ex}} \sum_{j=1}^{n_{A,k}} \sum_{i=1}^{n_{A_{j,k}}} \left( \log \left( [SEAP]_{A_{j,k}}^i \right) - \log \left( y_k(\mathbf{h}_k(\mathbf{p}), s_k, A_{j,k}) \right) \right)^2, \quad (\text{S34})$$

with  $n_{ex}$  denoting the number of experiments and  $s_k$  the scaling parameter for experiment  $k$ .  $y_k$  is the simulated observation of the experiment  $k$ , depending on the system function  $\mathbf{f}_k \in \{\mathbf{f}_{band}, \mathbf{f}_{low}, \mathbf{f}_{high}\}$  and on the parameter set  $\mathbf{h}_k(\mathbf{p})$ .

This function has to be optimized in respect to the dynamical parameters  $\mathbf{p}$  and the scaling parameters  $\mathbf{s}$ :

$$(\mathbf{p}, \mathbf{s})_{opt} = \arg \min_{(\mathbf{p}, \mathbf{s})} \chi^2(\mathbf{p}, \mathbf{s}) \quad (\text{S35})$$

The multi-experiment fit was performed with the experiments shown in Figure 1A-1C, Figure 2 and 3. The optimization of eq. (S35) leads to multiple optimal parameter sets. This means the parameters are not unique identifiable by the measured data.

One reason for this is that the solution of the ODE model is time dependent but the measured data are only at a single point in time. A second reason is the modular design of our systems. The overall output of the target gene depends on the outputs of the internal regulatory modules. But this measured overall output does not uniquely determine the parameters of the internal regulatory modules. However, with the different experiments we performed (e. g. Figure 1A and 1B) it is possible to identify the outputs of the internal modules. Combining these internal modules to different network structures, e.g. the low-detect with the high-detect filter (Figure 1C) or the auxin-dependent with the biotin-dependent band-detect filter (Figure 6), the resulting overall output depends only on the known outputs of the internal modules. This means, for the aim of this study it is not necessary to identify the exact biological parameters, but only a parameter set which can produce the output of each internal module. This parameter set is sufficient to make reliable predictions for different network structures which are constructed from of the internal regulatory modules.

Supplementary Table 1 shows such an exemplary parameter set that was used to produce the simulations in Figure 1A-1C, Figure 2 and 3. This parameter set was also

used to predict the further experiments, especially Figure 1D and Figure 6. Supplementary Table 2 contains the scaling parameters of the used experiments.

**Supplementary Table 1.** Chosen parameters for the auxin-dependent low-, high- and band-detect system obtained by a multi-experiment fit to the data shown in Figure 1A-1C, Figure 2 and 3.

Parameter	Value	Rescaling	Unit
$b'_1$	0.4373	$b_1/K_{m1}$	$h^{-1}$
$b_3$	0.0114	—	$U/L h^{-1}$
$k_1$	0.4932	—	$h^{-1}$
$k'_2$	0.4348	$k_2/K_{m1}$	$h^{-1}$
$k_3$	24.268	—	$(\mu M h)^{-1}$
$k_4$	0.0401	—	$h^{-1}$
$k_5$	96.206	—	$(\mu M h)^{-1}$
$k_6$	1.7202	—	$U/L h^{-1}$
$k'_7$	6.7594	$k_7[E-KRAB-AID]_0^2$	1
$K'_{m2}$	7.6526	$K_{m2}/K_{m1}$	1
$f$	0.0010	—	1
$K$	0.0407	—	$\mu M$
$[TIR1]_0$	0.0623	—	$\mu M$
$b_4$	0.7843	—	$U/L h^{-1}$

**Supplementary Table 2.** Scaling parameters obtained by a multi-experiment fit to the data shown in Figure 1A-1C, Figure 2 and 3.

Experiment	Parameter	Value
Low-detect filter, Figure 1A	$s_1$	0.1465
High-detect filter, Figure 1B	$s_2$	0.2516
Band-detect filter, Figure 1C	$s_3$	0.1463
Shape of band-detect filter, Figure 2B, blue line	$s_4$	0.9711
Shape of band-detect filter, Figure 2B, red line	$s_5$	1.0840
Shape of band-detect filter, Figure 2B, green line	$s_6$	0.8088
Shift of high-detect filter, Figure 3A, blue line	$s_7$	0.5368
Shift of high-detect filter, Figure 3A, red line	$s_8$	1.0105
Shift of low-detect filter, Figure 3B, blue line	$s_9$	2.4513
Shift of low-detect filter, Figure 3B, red line	$s_{10}$	0.2318
Shift of band-detect filter, Figure 3C, blue line	$s_{11}$	3.5015
Shift of band-detect filter, Figure 3C, red line	$s_{12}$	0.1683
Shape of band-detect filter, Figure 3D, red line	$s_{13}$	0.2763

### 3. Expanding the network

#### 3.1. Auxin-responsive band-detect filter based on ScbR

In the experiment shown in Figure 4 red line, tTA-AID is replaced by ScbR which is constitutively expressed. To describe this we have to modify eq. (S16a) and the parameters of eq. (S16c) because the target gene SEAP is expressed by a different promoter. The high-detect filter module is the same, thus we do not have to modify eq. (S16b):

$$\frac{d[ScbR]}{dt} = b_1^{ScbR} - (k_1^{ScbR} + k_3^{ScbR}[C]_{eq})[ScbR] \quad (S36a)$$

$$\frac{d[E-KRAB-AID]'}{dt} = k_4 - (k_4 + k_5[C]_{eq})[E-KRAB-AID]' \quad (S16b)$$

$$\frac{d[SEAP]}{dt} = b_3^{ScbR} + \frac{k_6^{ScbR}}{1+k_7'[E-KRAB-AID]'^2} \frac{[ScbR]^2}{K_{m2}^{ScbR^2} + [ScbR]^2} \quad (S36b)$$

The auxin-dependent band-detect filter is not restricted to the target gene SEAP. In Figure 4, blue line, we used luciferase as output. The system has the same structure thus, we only have to introduce new parameters in equation (S16c):

$$\frac{d[tTA-AID]'}{dt} = b_1' - (k_1 + k_3[C]_{eq})[tTA-AID]' + k_2' \frac{[tTA-AID]'^2}{1+[tTA-AID]'^2} \quad (S16a)$$

$$\frac{d[E-KRAB-AID]'}{dt} = k_4 - (k_4 + k_5[C]_{eq})[E-KRAB-AID]' \quad (S16b)$$

$$\frac{d[Luc]}{dt} = b_3^{luc} + \frac{k_6^{luc}}{1+k_7'[E-KRAB-AID]'^2} \frac{[tTA-AID]'^2}{K_{m2}^{luc^2} + [tTA-AID]'^2} \quad (S37)$$

Using the parameters obtained from the multi-experiment fit in the previous section and performing a fit of the additional parameters in the equations (S36a), (S36b) and (S37) to the data in Figure 4, we obtained the parameter shown in Supplementary Table 3.

**Supplementary Table 3.** Parameters used for the ScbR band-detect filter (Figure 4).

Parameter	Value	Unit
$b_3^{luc}$	0.1124	$U/L h^{-1}$
$k_6^{luc}$	1.0180	$U/L h^{-1}$
$K_{m2}^{luc}$	0.3891	1
$b_1^{ScbR}$	0.0781	$nMh^{-1}$
$b_3^{ScbR}$	0.0478	$U/L h^{-1}$
$k_1^{ScbR}$	0.0031	$h^{-1}$
$k_3^{ScbR}$	9.8441	$(\mu Mh)^{-1}$
$k_6^{ScbR}$	1.7380	$U/L h^{-1}$
$K_{m2}^{ScbR}$	42.703	$nM$

### 3.2. Biotin-responsive band-detect filter

The model for the biotin-dependent band-detect network is a simplified version from the model in Weber et al, 2007. The dilution due to cell growth and the RNA step in gene expression are neglected and the gene expression is described in the same way as in the auxin-dependent band-detect system. The expression of the target gene SEAP is described via Monod kinetic with PIP-streptavidin-biotin-VP16 complex (VBT) as activator. The concentration of biotin is denoted with  $[B]$ , avitag-VP16 with  $[V]$ , biotinylated VP16 with  $[VB]$  and the total intracellular concentration of avitag-VP16 with  $[V]_{tot}$ .

$$\frac{d[VB]}{dt} = p_1 \left( \frac{[B]}{K_{SB}+[B]} \right)^2 \left( \frac{[V]}{K_{SV}+[V]} \right) - p_2[VB] \quad (S38a)$$

$$\frac{d[SEAP]}{dt} = p_3 + p_4 \frac{[VBT]}{K_{ST}+[VBT]} \quad (S38b)$$

with  $[VBT] = \frac{p_5[VB]}{p_7[VB]+1+p_6[B]}$  (S38c)

and  $[V] = [V]_{tot} - [VB] - [VBT]$ . (S38d)

This model was fitted to the data shown in Figure 5, the used parameters are shown in Supplementary Table 4.

**Supplementary Table 4.** Used parameters of the simplified ODE model of the biotin-dependent band-detect filter.

Parameter	Value	Unit
$p_1$	16.7	$nM h^{-1}$
$p_2$	0.181	$h^{-1}$
$p_3$	0.0907	$U/L h^{-1}$
$p_4$	0.117	$U/L h^{-1}$
$p_5$	97.7	1
$p_6$	5.35	$nM^{-1}$
$p_7$	5.68	$nM^{-1}$
$K_{SB}$	63.3	$nM$
$K_{SV}$	14.9	$nM$
$K_{ST}$	0.131	$nM$
$[V]_{tot}$	3.18	$nM$

### 3.3. Two-dimensional gradients with the auxin-dependent band detect system

In Figure 1D we used the auxin-dependent band detect system to form two-dimensional gene expression patterns by using different auxin gradients. We performed a ring-shaped pattern and a delineation of one quadrant of the experimental space. To model this, we used the full band-detect model equations (S25) with the parameter set in Supplementary Table 1 and fitted only a new scaling parameter for each experiment.

$$[SEAP]_k = s_k [SEAP] \quad (S39)$$

The obtained scaling parameters are shown in Supplementary Table 5.

### 3.4. Additive superposition of biotin- and auxin-dependent band-detect filters

In Figure 6A we additively superposed the auxin- and biotin-dependent band-detect networks. For modeling we used the full models of each system equations (S25) and (S38) with the parameters from Supplementary Table 1 and 4:

$$\frac{d[tTA-AID]'}{dt} = b_1' - (k_1 + k_3[C]_{eq})[tTA-AID]' + k_2' \frac{[tTA-AID]'^2}{1+[tTA-AID]'^2} \quad (\text{S25a})$$

$$\frac{d[E-KRAB-AID]'}{dt} = k_4 - (k_4 + k_5[C]_{eq})[E-KRAB-AID]' \quad (\text{S25b})$$

$$\frac{d[SEAP]_a}{dt} = b_3 + \frac{k_6}{1+k_7'[E-KRAB-AID]'^2} \frac{[tTA-AID]'^2}{K_{m2}'^2 + [tTA-AID]'^2} \quad (\text{S25c})$$

$$\frac{d[VB]}{dt} = p_1 \left( \frac{[B]}{K_{SB} + [B]} \right)^2 \left( \frac{[V]}{K_{SV} + [V]} \right) - p_2[VB] \quad (\text{S38a})$$

$$\frac{d[SEAP]_b}{dt} = p_3 + p_4 \frac{[VBT]}{K_{ST} + [VBT]} \quad (\text{S38b})$$

$$\text{with} \quad [VBT] = \frac{p_5[VB]}{p_7[VB] + 1 + p_6[B]} \quad (\text{S38c})$$

$$\text{and} \quad [V] = [V]_{tot} - [VB] - [VBT]. \quad (\text{S38d})$$

Both systems work independently, thus we use as output of the superposed system the sum of the outputs of the single systems  $[SEAP]_a$  and  $[SEAP]_b$  with two scaling parameters  $\alpha_i$  and  $\beta_i$ :

$$[SEAP] = \alpha_i[SEAP]_a + \beta_i[SEAP]_b \quad (\text{S39})$$

The obtained scaling parameters from a fit to the data in Figure 6A are listed in Supplementary Table 5.

### 3.5. Conjunction-type connection of the biotin- and auxin-responsive band-detect networks

In Figure 6B we connected the output of the auxin- and biotin-dependent band-detect filter using a conjunction-type operation. This is accomplished by using as target gene two halves of split-firefly luciferase. To obtain an output signal both band-detect systems have to produce their part of the split-firefly luciferase. A simple way to implement this in a quantitative model is to take as output the product of the split-firefly luciferase parts, see eq. (S42). The used model is:

$$\frac{d[tTA-AID]'}{dt} = b_1' - (k_1 + k_3[C]_{eq})[tTA-AID]' + k_2' \frac{[tTA-AID]'^2}{1+[tTA-AID]'^2} \quad (S25a)$$

$$\frac{d[E-KRAB-AID]'}{dt} = k_4 - (k_4 + k_5[C]_{eq})[E-KRAB-AID]' \quad (S25b)$$

$$\frac{d[Luc_{aa155-245}]}{dt} = b_3 + \frac{k_6}{1+k_7'[E-KRAB-AID]'^2} \frac{[tTA-AID]'^2}{K_{m2}'^2 + [tTA-AID]'^2} \quad (S40)$$

$$\frac{d[VB]}{dt} = p_1 \left( \frac{[B]}{K_{SB} + [B]} \right)^2 \left( \frac{[V]}{K_{SV} + [V]} \right) - p_2[VB] \quad (S38a)$$

$$\frac{d[Luc_{aa1-155}]}{dt} = p_3 + p_4 \frac{[VBT]}{K_{ST} + [VBT]} \quad (S41)$$

with  $[VBT] = \frac{p_5[VB]}{p_7[VB] + 1 + p_6[B]}$  (S38c)

and  $[V] = [V]_{tot} - [VB] - [VBT]$ . (S38d)

$$[Luc] = \sigma [Luc_{aa1-155}] [Luc_{aa155-245}] \quad (S42)$$

This model has only one additional parameter  $\sigma$  which was fitted to the data shown in Figure 6B. The resulting parameter is shown in Supplementary Table 5.

### 3.6. Direct rewiring of the auxin-responsive low-detect filter with the biotin-responsive band-detect network.

In the experiment shown in Figure 6C, we interconnected the auxin-responsive low-detect filter with the biotin-responsive band-detect network directly by coupling the

avitag-VP16 from the biotin-dependent system to the auxin-dependent system. This is done by fusing the degron domain AID to avitag-VP16. Additionally the avitag-VP16 expression is controlled by the  $P_{TET}$  promoter with the transcription factor tTA-AID. The auxin-dependent band-detect system was not modified, thus, we use for modeling the auxin-dependent part eq. (S25) with the parameter from Supplementary Table 1:

$$\frac{d[tTA-AID]'}{dt} = b_1' - (k_1 + k_3[C]_{eq})[tTA-AID]' + k_2' \frac{[tTA-AID]'^2}{1+[tTA-AID]'^2} \quad (S25a)$$

$$\frac{d[E-KRAB-AID]'}{dt} = k_4 - (k_4 + k_5[C]_{eq})[E-KRAB-AID]' \quad (S25b)$$

$$\frac{d[SEAP]_a}{dt} = b_3 + \frac{k_6}{1+k_7'[E-KRAB-AID]'^2} \frac{[tTA-AID]'^2}{K_{m2}' + [tTA-AID]'^2} \quad (S25c)$$

Since the avitag-VP16 is not expressed constitutively, we have to introduce an ODE eq. (S43b) for the total amount of avitag-VP16  $[V_{tot}]$  which is under control of tTA-AID via Monod kinetics and is degraded by the auxin-TIR1 complex C. It is assumed that the biotinylated VP16 is also actively degraded by the auxin-TIR1 complex C so the equation for VB needs also an additional degradation term, see eq. (S43a). This leads to the model:

$$\frac{d[VB]}{dt} = p_1 \left( \frac{[B]}{K_{SB}+[B]} \right)^2 \left( \frac{[V]}{K_{SV}+[V]} \right) - (p_2 + k_{v2}[C]_{eq})[VB] \quad (S43a)$$

$$\frac{d[V_{tot}]}{dt} = b_v + k_{v1} \frac{[tTA-AID]'^2}{K_{mv} + [tTA-AID]'^2} - (p_2 + k_{v2}[C]_{eq})[V_{tot}] \quad (S43b)$$

$$\frac{d[SEAP]_b}{dt} = p_3 + p_4 \frac{[VBT]}{K_{ST}+[VBT]} \quad (S38b)$$

with  $[VBT] = \frac{p_5[VB]}{p_7[VB]+1+p_6[B]}$  (S38c)

and  $[V] = [V]_{tot} - [VB] - [VBT]$ . (S38d)

The outputs of both systems are added with some scaling parameters  $\alpha_3$  and  $\beta_3$  to the overall output of the interconnected system:

$$[SEAP] = \alpha_3[SEAP]_a + \beta_3[SEAP]_b \quad (S43c)$$

To simulate this model, the parameter from Supplementary Table 1 and 4 were used and the additional parameters in eq. (S43a)-(S43c) were fitted to the data shown in Figure 6C. The obtained parameters are shown in Supplementary Table 5.

**Supplementary Table 5.** Used parameters for the experiments in Figure 1D and 6A-6C.

Experiment	Description	Parameter	Value
Ring-shaped pattern, Figure 1D	Scaling parameter	$s_{13}$	0.1506
Upper left quadrant, Figure 1D	Scaling parameter	$s_{14}$	0.1797
Parallel superposition, Figure 6A	Scaling of auxin-dependent part	$\alpha_1$	0.2105
Parallel superposition, Figure 6A	Scaling of biotin-dependent part	$\beta_1$	0.3371
Orthogonal superposition, Figure 6A	Scaling of auxin-dependent part	$\alpha_2$	0.1509
Orthogonal superposition, Figure 6A	Scaling of biotin-dependent part	$\beta_2$	0.2403
Connection by AND gate in the output, Figure 6B	Product of split luciferase binding strength and scaling factor	$\sigma$	0.1199
Direct interconnection, Figure 6C	Basal production of VP16	$b_v$	1.065
Direct interconnection, Figure 6C	Production of VP16	$k_{v1}$	0.9387
Direct interconnection, Figure 6C	Auxin-induced degradation of VP16	$k_{v2}$	100.37
Direct interconnection, Figure 6C	$K_m$ value of monod kinetic of VP16 expression	$K_{mv}$	4.1250
Direct interconnection, Figure 6C	Scaling of auxin-dependent part	$\alpha_3$	0.0829
Direct interconnection, Figure 6C	Scaling of biotin-dependent part	$\beta_3$	0.0670

## 4. Auxin and biotin gradients

The auxin and biotin concentration courses in the experiment emulate a gradient as formed by a diffusion process. The diffusion of a substance with the concentration  $p(x, t)$  on a one-dimensional spatial domain  $x \in [0, x_{max}]$  is described by the diffusion equation

$$\frac{dp(t,x)}{dt} = D \frac{d^2p(t,x)}{dx^2}, \quad (\text{S44})$$

with the diffusion coefficient  $D$ . Assuming as initial condition a source at  $x = 0$  the solution of eq. (S44) has the form

$$p(t, x) = \frac{a}{\sqrt{4\pi Dt}} e^{\frac{-x^2}{4Dt}}, \quad (\text{S45})$$

the constant  $a$  is proportional to the amount of substance at  $t = 0$  (Evans, 2002). This is a Gaussian function which is becoming broader with increasing time  $t$ . For the morphogen gradients used in this study we took one snapshot of this distribution  $p(t, x)$  at a fixed time point  $\tilde{t}$ . This leads to

$$p(x) = A e^{\frac{-x^2}{s}}, \quad (\text{S46})$$

with  $A = \frac{a}{\sqrt{4\pi D\tilde{t}}}$  and  $s = 4D\tilde{t}$ .

For the auxin concentrations used in the experiments shown in Figure 1A-1C, 2, 3 and 4 we used  $A = 200 \mu\text{M}$  and  $s = 6.8 \text{ cm}^2$ . In the biotin-dependent band-detect network (Figure 5B) the biotin gradient was produced with  $A = 20000 \text{ nM}$  and  $s = 2 \text{ cm}^2$ .

In the first experiment in Figure 1D a dome-shaped gradient was used. This corresponds to a source in the middle of the domain. The auxin gradient used in the second experiment shown in Figure 1D (lower panel) is a superposition of two orthogonal gradients

$$[AUX](x, y) = Ae^{-x^2/s} + Ae^{-y^2/s}. \quad (\text{S47})$$

This corresponds to a source on the left and the upper edge. Both gradients were produced with the parameters  $A = 200 \mu\text{M}$  and  $s = 4.4 \text{ cm}^2$ . In the experiments shown in Figure 6A two different morphogens were used. In the first experiment auxin has its maximum on the left edge and biotin on the right edge. This leads to

$$[AUX](x, y) = Ae^{-x^2/s_A} \quad (\text{S48a})$$

$$[B](x, y) = Be^{-(x-11)^2/s_B}. \quad (\text{S48b})$$

As parameter we used  $A = 200 \mu\text{M}$ ,  $B = 20000 \text{ nM}$ ,  $s_A = 1.1 \text{ cm}^2$  and  $s_B = 2 \text{ cm}^2$ .

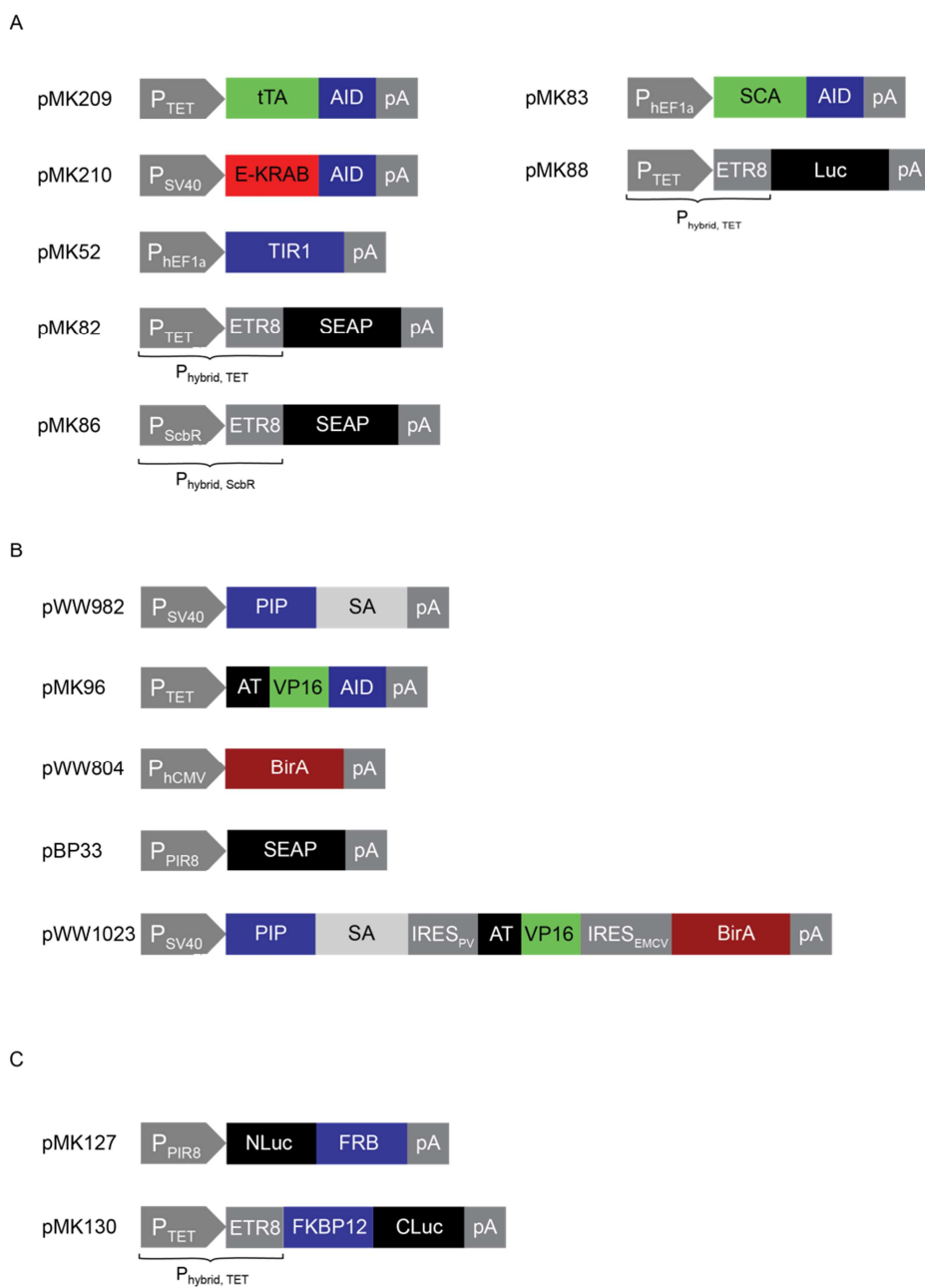
In the second experiment of Figure 6A and in the experiments shown in Figure 6B-6C the auxin and biotin gradient were chosen orthogonal. The source of the auxin gradient is on the right edge. Biotin has its source on the lower edge. The gradients are obtained by the equations

$$[AUX](x, y) = Ae^{-(x-11)^2/s_A} \quad (\text{S49a})$$

$$[B](x, y) = Be^{-(y-7)^2/s_B}, \quad (\text{S49b})$$

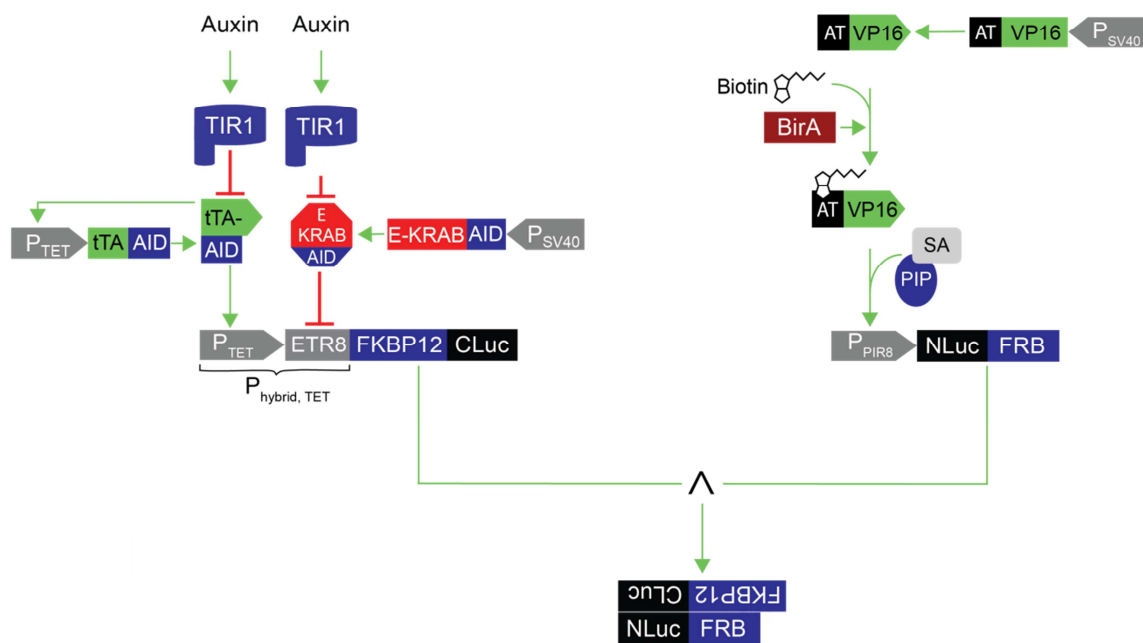
with  $A = 200 \mu\text{M}$ ,  $B = 20000 \text{ nM}$  and  $s_A = 6.8 \text{ cm}^2$  and  $s_B = 2 \text{ cm}^2$ .

## 5. Supplementary Figures

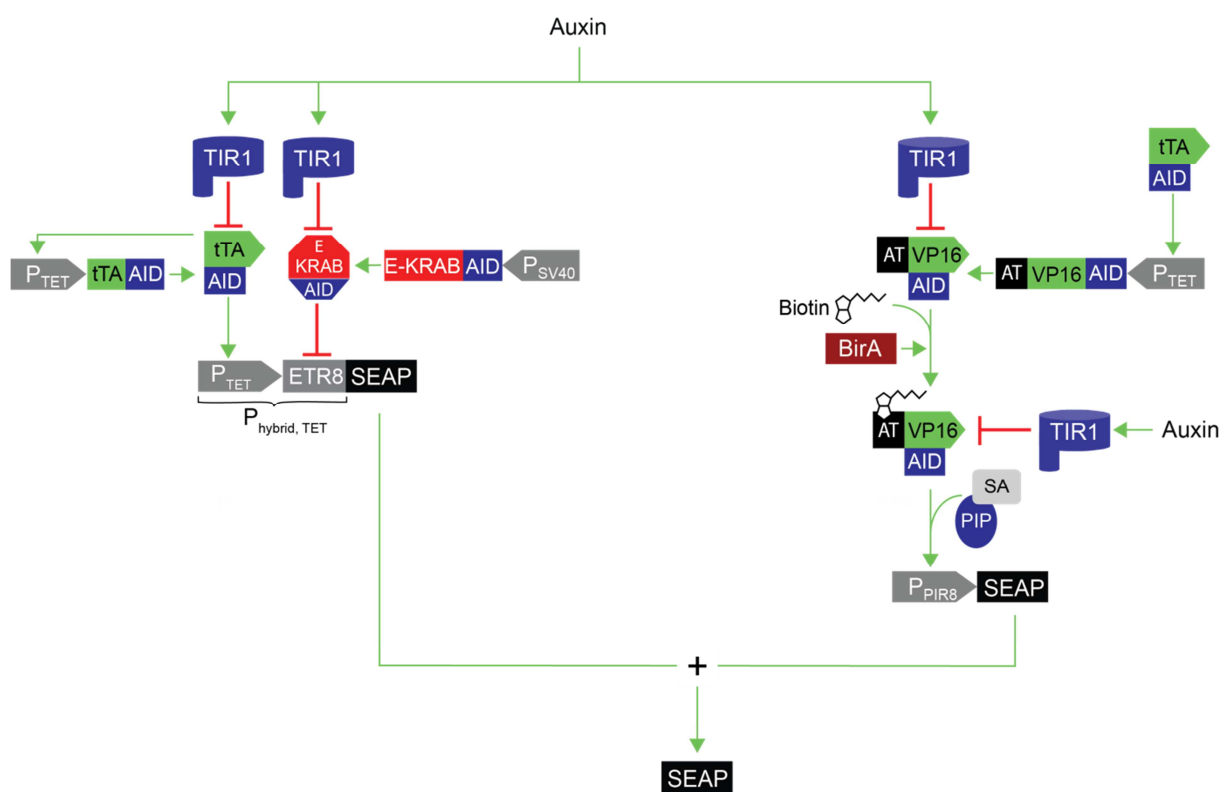


**Supplementary Figure 1.** Schematic illustration of vectors used in this study. **(A)** Vectors for the auxin-responsive band-detect network. **(B)** Vectors for the biotin-responsive band-detect networks. **(C)** Output vectors for the combined auxin- and biotin-responsive networks. Abbreviations: AID, auxin-inducible degradation domain; AT, Avitag biotinylation sequence; BirA, *E.coli* biotin ligase; CLuc, C-terminal fragment of the split-firefly luciferase; E-KRAB, erythromycin-dependent

transsilencer; ETR8, octameric operator sites of the macrolide-dependent repressor E; FKBP12, FK506-binding protein 12; FRB, FKBP12-rapamycin-binding domain; IRES<sub>EMCV</sub>, internal ribosomal entry site from encephalomyocarditis virus; IRES<sub>PV</sub>, internal ribosome entry site of polioviral origin; Luc, firefly luciferase; NLuc, N-terminal fragment of the split-firefly luciferase; pA, polyadenylation signal; P<sub>hCMV</sub>, human cytomegalovirus-derived constitutive promoter; P<sub>hEF1 $\alpha$</sub> , constitutive promoter from human elongation factor 1 $\alpha$ ; P<sub>hybrid, ScbR</sub>, SCA-AID- and E-KRAB-AID-responsive hybrid promoter; P<sub>hybrid, TET</sub>, tTA-AID- and E-KRAB-AID-responsive hybrid promoter; PIP, streptogramin-dependent repressor; P<sub>PIR8</sub> PIP-specific promoter; P<sub>SV40</sub> simian virus 40-derived constitutive promoter; P<sub>TET</sub>, tTA-responsive promoter; SA, streptavidin; SCA, *Streptomyces coelicolor*-derived transactivator; SEAP, secreted alkaline phosphatase; TIR1, auxin co-receptor transport inhibitor response 1; tTA, tetracycline-dependent transactivator; VP16, *Herpes simplex*-derived transactivation domain.



**Supplementary Figure 2.** Connectivity diagram of the auxin- and biotin-responsive band-detect networks interconnected by conjunction. The output promoters of the auxin- and biotin-responsive band-detect filters were connected to split firefly luciferase (CLuc and NLuc) fused to the FKBP12-FRB heterodimerization system. Only upon dimerization of the two modules, CLuc-FKBP12 and NLuc-FRB, active luciferase is reconstituted. For abbreviations see Supplementary Figure 1.



**Supplementary Figure 3.** Connectivity diagram of the directly rewired auxin- and biotin-responsive networks. The auxin-responsive low-detect network was rewired to the biotin-responsive band-detect network in a conjunction-type manner by fusing the auxin-inducible degradation domain AID to the biotin-responsive transactivation domain avitag-VP16 (AT-VP16). This system was additively connected to the auxin-responsive band-detect network by the introduction of the hybrid promoter  $P_{\text{hybrid, TET}}$  driving SEAP expression. For abbreviations see Supplementary Figure 1.

## 6. Supplementary Data Tables

**Supplementary Table 6.** Experimental data and simulation results of the experiments in Figure 1D in SEAP activity (U/L). (A) Experimental data of ring-shaped pattern, (B) simulation of ring-shape pattern, (C) experimental data of two orthogonally overlapping gradients, (D) simulation of two orthogonally overlapping gradients.

**A**

0.713	0.493	0.648	0.619	0.630	0.662	0.745
0.536	2.147	2.687	2.752	2.753	2.199	0.868
0.553	2.346	0.461	0.407	0.383	2.646	0.639
0.792	2.199	0.157	0.058	0.246	3.054	0.783
0.647	2.725	0.536	0.434	0.387	2.958	0.729
0.594	2.517	2.990	3.082	3.032	2.284	0.749
0.833	0.549	0.706	0.626	0.709	0.756	0.703

**B**

0.954	0.954	0.954	0.954	0.954	0.954	0.954
0.954	1.441	1.814	1.814	1.814	1.441	0.954
0.954	1.814	0.250	0.250	0.250	1.814	0.954
0.954	1.814	0.250	0.203	0.250	1.814	0.954
0.954	1.814	0.250	0.250	0.250	1.814	0.954
0.954	1.441	1.814	1.814	1.814	1.441	0.954
0.954	0.954	0.954	0.954	0.954	0.954	0.954

**C**

0.343	0.254	0.199	0.213	0.174	0.272	0.344	0.310	0.237	0.222	0.244	0.345
0.310	0.225	0.217	0.207	0.217	0.255	0.356	0.280	0.263	0.206	0.278	0.284
0.298	0.279	0.208	0.319	0.354	0.597	0.598	0.556	0.406	0.364	0.486	0.562
0.270	0.224	0.284	0.545	0.805	0.753	2.899	1.366	1.797	1.290	1.213	1.980
0.238	0.182	0.286	0.546	1.306	1.597	4.638	4.200	4.150	3.951	3.578	4.423
0.328	0.161	0.438	0.706	1.273	0.857	2.371	1.474	1.468	1.360	1.486	1.722
0.329	0.386	0.445	1.328	2.717	1.484	0.557	0.308	0.366	0.328	0.356	0.467
0.316	0.366	0.423	1.719	3.736	2.511	0.429	0.413	0.385	0.316	0.449	0.383

**D**

0.217	0.219	0.227	0.236	0.241	0.243	0.243	0.243	0.243	0.243	0.243	0.243
0.219	0.223	0.233	0.247	0.256	0.258	0.259	0.259	0.259	0.259	0.259	0.259
0.227	0.233	0.258	0.305	0.342	0.355	0.355	0.355	0.355	0.355	0.355	0.355
0.236	0.247	0.305	0.491	0.774	0.876	0.905	0.905	0.905	0.905	0.905	0.905
0.241	0.256	0.342	0.774	1.674	2.092	2.164	2.164	2.164	2.164	2.164	2.164
0.243	0.258	0.355	0.876	2.092	1.719	1.558	1.558	1.558	1.558	1.558	1.558
0.243	0.259	0.355	0.905	2.164	1.558	1.195	1.164	1.164	1.164	1.164	1.170
0.243	0.259	0.355	0.905	2.164	1.558	1.164	1.132	1.130	1.130	1.130	1.130

**Supplementary Table 7.** Experimental data and simulation results of the experiments in Figure 6A in SEAP activity (U/L). (A) Experimental data of two parallel auxin and biotin gradients, (B) simulation of two parallel auxin and biotin gradients, (C) experimental data of two orthogonal auxin and biotin gradients, (D) simulation of two orthogonal auxin and biotin gradients.

**A**

2.125	2.093	4.392	2.774	2.899	2.918	3.309	3.084	3.982	3.067	2.683	2.735
1.594	2.140	4.190	2.717	2.842	2.918	3.357	3.105	4.449	3.085	2.482	2.535
1.950	2.356	4.533	2.800	3.145	3.114	3.613	2.968	4.203	3.013	2.569	2.511
1.596	2.304	3.956	2.720	2.936	2.753	3.558	2.759	4.185	2.954	2.797	2.771
1.976	1.990	3.999	2.568	2.875	3.120	3.133	3.298	3.997	2.804	2.453	2.394
1.498	2.155	3.766	2.656	2.744	2.770	3.073	2.730	4.055	2.779	2.556	2.319
1.853	2.038	4.487	2.446	2.982	3.085	3.210	2.514	4.022	2.696	2.783	2.602
1.902	2.170	3.986	2.687	2.754	3.159	3.191	3.341	4.237	2.684	2.747	2.622

**B**

1.752	1.885	3.983	2.829	2.790	2.790	2.812	4.378	3.992	3.050	2.855	2.830
1.752	1.885	3.983	2.829	2.790	2.790	2.812	4.378	3.992	3.050	2.855	2.830
1.752	1.885	3.983	2.829	2.790	2.790	2.812	4.378	3.992	3.050	2.855	2.830
1.752	1.885	3.983	2.829	2.790	2.790	2.812	4.378	3.992	3.050	2.855	2.830
1.752	1.885	3.983	2.829	2.790	2.790	2.812	4.378	3.992	3.050	2.855	2.830
1.752	1.885	3.983	2.829	2.790	2.790	2.812	4.378	3.992	3.050	2.855	2.830
1.752	1.885	3.983	2.829	2.790	2.790	2.812	4.378	3.992	3.050	2.855	2.830
1.752	1.885	3.983	2.829	2.790	2.790	2.812	4.378	3.992	3.050	2.855	2.830

**C**

1.699	1.682	1.619	1.784	1.836	2.793	4.404	2.315	1.961	1.310	1.224	1.372
1.655	1.568	1.662	1.628	1.897	3.391	4.394	2.529	1.588	1.054	1.255	1.325
1.463	1.632	1.330	1.325	1.799	2.757	4.201	2.402	1.571	1.403	1.367	1.501
2.677	3.167	2.713	3.192	3.570	4.453	5.850	4.294	3.573	3.143	2.835	3.114
2.212	2.353	2.224	2.611	2.804	3.745	4.474	3.404	2.816	2.603	2.777	2.628
1.603	1.651	1.611	1.850	1.685	3.349	4.462	2.732	1.641	1.582	1.396	1.457
1.599	1.623	1.562	1.603	1.577	3.074	4.182	2.497	1.707	1.368	1.098	1.263
1.419	1.849	1.569	1.495	2.017	3.122	4.194	2.849	1.563	1.262	1.120	0.639

**D**

1.994	1.994	1.994	2.002	2.070	2.490	2.861	2.033	1.451	1.297	1.258	1.250
1.994	1.994	1.994	2.002	2.070	2.490	2.861	2.033	1.451	1.297	1.258	1.250
2.010	2.010	2.010	2.018	2.086	2.506	2.877	2.049	1.467	1.313	1.274	1.266
3.126	3.126	3.127	3.134	3.202	3.622	3.993	3.165	2.584	2.429	2.390	2.382
2.851	2.851	2.852	2.859	2.927	3.347	3.718	2.890	2.309	2.154	2.116	2.108
2.180	2.180	2.180	2.188	2.256	2.676	3.047	2.219	1.637	1.483	1.444	1.436
2.041	2.041	2.041	2.049	2.117	2.537	2.908	2.080	1.498	1.344	1.305	1.297
2.023	2.023	2.023	2.031	2.099	2.519	2.890	2.062	1.480	1.326	1.287	1.279

**Supplementary Table 8.** Experimental data and simulation results of the experiment shown in Figure 6B in luciferase activity (Rlu, relative light units). (A) Experimental data, (B) simulation results.

**A**

2.602	2.989	3.522	3.470	3.657	5.978	5.446	4.857	3.034	1.912	1.602	1.234
3.325	3.074	3.546	3.679	4.027	6.036	5.324	6.821	3.171	1.949	1.761	1.398
4.038	3.317	3.512	3.853	3.937	6.266	6.266	5.963	2.854	1.737	1.420	1.300
2.249	2.091	2.788	3.292	3.463	7.538	8.787	6.570	3.284	2.132	1.692	1.697
2.323	2.848	2.552	2.761	2.994	7.295	8.460	5.775	2.699	1.715	1.495	1.345
2.524	2.458	2.715	2.263	2.519	4.513	5.785	6.463	2.026	1.948	1.385	1.356
1.705	2.506	2.359	2.401	2.384	3.967	6.174	4.763	2.505	1.689	1.241	1.246
1.979	2.124	2.169	2.173	2.394	3.794	4.829	4.707	1.983	1.262	1.048	1.059

**B**

3.279	3.279	3.281	3.308	3.543	4.997	6.281	3.414	1.401	0.866	0.733	0.705
3.279	3.279	3.281	3.308	3.543	4.997	6.281	3.414	1.401	0.866	0.733	0.705
3.329	3.329	3.332	3.359	3.597	5.073	6.377	3.466	1.423	0.880	0.744	0.716
6.826	6.827	6.831	6.887	7.377	10.403	13.077	7.107	2.918	1.804	1.526	1.468
5.965	5.966	5.970	6.018	6.446	9.091	11.427	6.211	2.549	1.576	1.333	1.283
3.862	3.862	3.864	3.896	4.173	5.885	7.397	4.020	1.650	1.020	0.863	0.831
3.426	3.426	3.428	3.456	3.702	5.221	6.562	3.567	1.464	0.905	0.766	0.737
3.369	3.369	3.372	3.399	3.641	5.135	6.454	3.508	1.440	0.890	0.753	0.725

**Supplementary Table 9.** Experimental data and simulation results of the experiment shown in Figure 6C in SEAP activity (U/L). (A) Experimental data, (B) simulation results.

**A**

1.415	1.388	1.221	1.109	1.121	1.959	2.322	0.706	0.444	0.179	0.241	0.281
1.355	0.839	0.814	1.135	1.177	1.409	1.976	0.569	0.333	0.167	0.161	0.261
1.308	1.100	0.986	1.162	1.282	1.602	2.930	0.698	0.339	0.302	0.276	0.353
2.880	2.916	2.947	2.574	2.335	3.041	3.320	0.842	0.270	0.142	0.212	0.251
2.607	2.158	2.198	2.033	2.264	2.356	2.616	1.079	0.381	0.248	0.221	0.255
0.804	0.967	0.985	1.020	1.098	1.320	1.904	0.510	0.265	0.181	0.175	0.149
0.802	0.857	1.080	1.132	1.078	1.440	2.138	0.624	0.243	0.195	0.139	0.146
0.794	1.381	1.065	0.765	1.299	1.769	2.571	0.555	0.208	0.153	0.141	0.130

**B**

0.812	0.812	0.813	0.817	0.854	1.085	1.289	0.834	0.514	0.429	0.408	0.404
0.812	0.812	0.813	0.817	0.854	1.085	1.289	0.834	0.514	0.429	0.408	0.404
0.814	0.814	0.814	0.818	0.855	1.086	1.289	0.834	0.514	0.429	0.408	0.404
1.079	1.079	1.079	1.083	1.116	1.323	1.428	0.869	0.523	0.433	0.411	0.406
1.063	1.063	1.063	1.067	1.101	1.311	1.437	0.885	0.529	0.437	0.414	0.409
0.879	0.879	0.879	0.883	0.918	1.136	1.313	0.840	0.516	0.430	0.409	0.405
0.830	0.830	0.830	0.834	0.871	1.098	1.294	0.835	0.515	0.430	0.408	0.404
0.823	0.823	0.824	0.828	0.865	1.093	1.292	0.835	0.515	0.430	0.408	0.404

## 7. Supplementary References

Evans LC (2002) Partial Differential Equations. Graduate Studies in Mathematics **19**. American Mathematical Society 44-47

Fussenegger M, Morris RP, Fux C, Rimann M, von Stockar B, Thompson CJ, Bailey JE (2000) Streptogramin-based gene regulation systems for mammalian cells. *Nat Biotechnol* **18**(11): 1203-1208

Karlebach G, Shamir R (2008) Modelling and analysis of gene regulatory networks. *Nat Rev Mol Cell Bio* **9**: 770-780

Koch AL (1966) The logarithm in biology. 1. Mechanisms generating the log-normal distribution exactly. *J Theor Biol* **12**(2): 276-290

Kramer BP, Viretta AU, Daoud-El Baba M, Aubel D, Weber W, Fussenegger M (2004) An engineered epigenetic transgene switch in mammalian cells. *Nat Biotechnol* **22**: 867-870

Kreutz C, Bartolome Rodriguez MM, Maiwald T, Seidl M, Blum HE, Mohr L, Timmer J (2007) An error model for protein quantification. *Bioinformatics* **23**(20): 2747-2753

Raue A, Kreutz C, Maiwald T, Bachmann J, Schilling M, Klingmüller U, Timmer J (2009) Structural and practical identifiability analysis of partially observed dynamical models by exploiting the profile likelihood. *Bioinformatics* **25**(15): 1923-1929

Weber W, Stelling J, Rimann M, Keller B, Daoud-El Baba M, Weber CC, Aubel D, Fussenegger M (2007) A synthetic time-delay circuit in mammalian cells and mice. *Proc Natl Acad Sci U S A* **104**: 2643-2648